PHYSICAL REVIEW B **77**, 121401(R) (2008)

Exceptional surface stability in late transition metal alloys driven by lattice strain

L. Vitos,[1,2,3] M. Ropo,[4,5] K. Kokko,[4] M. P. J. Punkkinen,[4] J. Kollár,[3] and B. Johansson[1,2]
[1]*Applied Materials Physics, Department of Materials Science and Engineering, Royal Institute of Technology, SE-10044 Stockholm, Sweden*
[2]*Condensed Matter Theory Group, Physics Department, Uppsala University, S-75121 Uppsala, Box 530, Sweden*
[3]*Research Institute for Solid State Physics and Optics, Budapest H-1525, P.O. Box 49, Hungary*
[4]*Department of Physics, University of Turku, FIN-20014 Turku, Finland*
[5]*Graduate School of Materials Research, Turku, Finland*
(Received 5 February 2008; published 6 March 2008)

Due to the lower compressibility of the close-packed crystallographic planes compared to the less close-packed ones, the open free surfaces of the late transition and noble metals are generally expected to become thermodynamically stable with increasing pressure. Surface segregation in concentrated alloys and heteroepitaxial growth are possible mechanisms to create additional lattice strain around the surface layer and, thus, alter the surface stability at ambient conditions. Here we demonstrate this phenomenon in the case of PdAg random alloys by performing *ab initio* density functional calculations for the surface energy and stress. Our findings reveal anomalous surface stability, so far experienced only in some magnetic transition metals, and exceptionally large excess surface stress as an indicator for surface reconstruction.

DOI: 10.1103/PhysRevB.77.121401 PACS number(s): 68.03.Cd, 71.15.Nc, 82.45.Jn

Metal surfaces play the key role in catalytic, tribological, epitaxial growth and nanocluster phenomena, and therefore their experimental exploration and theoretical description have always been in the focus of materials science.[1–3] The surface chemistry is the primary effect governing the surface reactivity, whereas the surface morphology, surface orientation and flatness, degree of roughness, and surface reconstruction are of fundamental importance on the constitution and reactivity of metallic nanoparticles, on atomic friction and interfacial cohesion, as well as on epitaxial heterostructures.[4,5]

The thermodynamical stability of different crystallographic surfaces is determined by the surface energy (γ), defined as the surface excess free energy per unit area. Except for the body centered cubic (bcc) nonmagnetic transition metals and some alkaline metals, the surface energies of metals exhibit a strong orientation dependence.[6–8] According to the simple broken-bond model, the close-packed surfaces, i.e., those with the lowest roughness,[9] should possess the lowest surface energy. This trend is well obeyed by the face centered cubic (fcc) transition and noble metals.[6] The only striking anomalies that have been found so far are in bcc Cr and Fe, where surface magnetism stabilizes the (100) facet instead of the close-packed (110) facet.[10,11]

Another fundamental surface parameter is the surface stress (τ), representing the atomic-level in-plane force acting in the surface region.[1,2,12,13] It plays a decisive role in a wide variety of surface phenomena.[2] In particular, the excess surface stress ($\tau-\gamma$) is identified as the driving force for the reconstruction in the microscopic modeling.[1] According to the continuum model by Herring[14] and Cammarata,[15] the stability criterion for metal surfaces requires that the absolute value of the excess surface stress should be at least one order of magnitude smaller than the elastic strain energy associated with the surface reconstruction. Recently, Kwon *et al.*[13] presented a systematic theoretical study of the surface energy and stress of 4*d* transition metals. In good agreement with observations, the calculated excess surface stresses for all the (111) and (100) fcc surfaces were found to be small, predicting the stability of these 4*d* transition-metal surfaces.

In this Rapid Communication, using a computational approach based on first-principles alloy theory, we investigate the above surface properties in the case of late transition-metal alloys. For concreteness, we consider the palladium-silver alloy forming continuous solid solution in the fcc structure. However, the disclosed phenomena are expected to be valid for any binary transition-metal solid solution and also epitaxial heterostructure with sizable lattice mismatch. By computing the surface energy and surface stress of PdAg random alloys as a function of bulk composition, here we demonstrate that lattice strain can reverse the usual surface anisotropy, and can lead to anomalously large excess surface stress.

The present calculations were carried out using the density functional theory[16] formulated within the local density approximation[17,18] for the exchange-correlation functional. For nonmagnetic late-transition metals and transition-metal surfaces, this approximation turned out to be superior compared to the gradient corrected functionals.[6,19,20] The Kohn-Sham equations were solved using the exact muffin-tin orbitals (EMTO) method,[21–24] and the substitutional disorder was taken into account using the coherent potential approximation (CPA)[25,26] as implemented in the EMTO-CPA method.[27] The order-disorder transition temperature in PdAg has been predicted to be around 340 K in Ag-rich alloys and 240 K in Pd-rich alloys.[29] Calculations based on the screened generalized perturbation method[30] have shown that above these temperatures, the surface of PdAg is adequately described by the present single-site mean-field approximation.

Our study focuses on the (111) and (100) surfaces of the fcc PdAg alloys. The two surfaces were modeled using slabs consisting of 8 atomic layers parallel to the (111) and (100) crystallographic facets, respectively. The slabs were separated by vacuum layers having a width equivalent with four atomic layers. First, the intralayer and interlayer (λ_{ij}, i, and j

TABLE I. Calculated bulk lattice constant (a in Å), theoretical equilibrium Ag concentrations in the subsurface layer (c^2) (Ref. 31), and the excess surface stress (in mJ/m^2) for the (111) and (100) facets of PdAg alloys as a function of Ag content in the bulk (c). Asterisks mark the surfaces which are estimated (Ref. 15) to be unstable against reconstruction.

c	a	c^2	$(\tau-\gamma)_{111}$	$(\tau-\gamma)_{100}$
0.0	3.854	-	1.07	0.54
0.1	3.867	0.00	2.01*	1.98*
0.2	3.884	0.00	1.67*	1.63*
0.3	3.899	0.00	1.32*	1.29*
0.4	3.913	0.00	1.02	1.02
0.5	3.928	0.02	0.80	0.63
0.6	3.943	0.41	0.78	0.49
0.7	3.958	0.57	0.64	0.46
1.0	4.016	1.00	0.41	0.16

are the layer indices) lattice constants were fixed to the corresponding bulk values obtained from the theoretical cubic lattice constants (Table I). Then, the relaxed surface geometry was determined by optimizing the distance between the top layer and the subsurface layer (λ_{12}) while keeping all the other positions unchanged. The EMTO-CPA calculations[28] were performed for pure Pd and Ag, and for $Pd_{1-c}Ag_c$ alloys with $c=0.1,0.2,\ldots,0.7$. The concentrations of the four central layers from the slabs were fixed to the corresponding bulk value. For the concentrations of the top layer (c^1) and subsurface layer (c^2) we used the previously determined low-temperature values,[31] which have been found to agree well with the experimental data.[32] Since at temperatures below ~600 K, the two fcc surfaces in question have similar concentration profiles, here for both facets we used the average values $c^1=1$ and c^2 listed in Table I as a function of c.

Surface relaxation. The surface energy of a close-packed metal surface shows a weak layer relaxation dependence. At the same time, the surface stress has been found[13] to depend nearly linearly on λ_{ij}, which makes the geometry optimization an indispensable first step in stress calculation. The present theoretical top-layer relaxations, defined as $\delta_{12} \equiv (\lambda_{12}^s-\lambda_{12}^b)/\lambda_{12}^b$, with λ_{12}^s and λ_{12}^b being the equilibrium surface and bulk interlayer distance, respectively, are displayed in the inset of Fig. 1. The (111) surface shows small outward relaxations characteristic to the close-packed surfaces of Pd and Ag,[13] with a slight maximum near $c=0.1$. The (100) surface exhibits a more nonuniform behavior: it relaxes inward in Pd- and in Ag-rich PdAg alloys, but in Pd-rich alloys we can see almost zero or slightly positive relaxation. The obtained trend for $\delta_{12}(c)$ is a direct consequence of the lattice mismatch strain. Due to the ~4% difference between Pd and Ag lattice constants, the pure Ag surface layer on PdAg substrate is subject of an increasing strain as going from the Ag end to the Pd-rich end. In the Pd-rich alloys, part of this strain can be released by outward surface relaxation, which increases the average volume of the surface Ag atoms.

Surface energy. The surface energy was obtained from the difference between the slab and bulk grand potentials, viz.

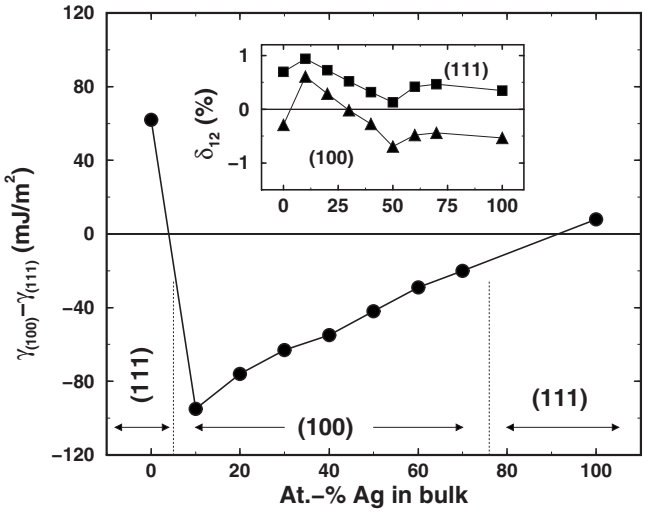

FIG. 1. Difference between the surface energies for the (100) and (111) surfaces of the PdAg alloys as a function of bulk Ag content. Negative numbers indicate that the (100) facet is more stable than the (111) facet. The approximate stability fields of the two surfaces are indicated by arrows. Inset shows the top-layer relaxations for the (100) and (111) facets as a function of bulk Ag content.

$$\gamma = \frac{E^s(c^1,c^2,c) - 8E^b(c) - \mu^b \sum_{i=1}^{2} (c^i - c)}{2A}. \qquad (1)$$

Here $E^s \equiv E^s(\lambda_{12}^s)$ is the equilibrium slab energy, the bulk energy E^b refers to one formula unit, A is the surface area, $\mu^b = \partial E^b(c)/\partial c$ is the bulk effective chemical potential, and the factor 2 appears because of the two surfaces per slab. Since we are mostly interested in the difference between γ_{100} and γ_{111}, in Eq. (1) the entropy terms have been omitted. The numerical error in the calculated γ, estimated from the finite slab size and Brillouin zone sampling, is less than 10 mJ/m^2.

Figure 1 shows the surface energy difference $\Delta\gamma \equiv \gamma_{100} - \gamma_{111}$ as a function of bulk Ag concentration. The present surface energies for Pd and Ag are 2.37 and 1.42 J/m^2 for the (111) surface, and 2.43 and 1.43 J/m^2 for the (100) surface. Thus, for the end members, the (111) facet is found to be the stable surface, in good agreement with former studies.[6,13,33] With Pd addition, we find that the (100) facet is stabilized against the most close-packed (111) facet. Taking into account our numerical uncertainties, we come to the unexpected conclusion that in Pd-rich PdAg alloys the (100) facet is the thermodynamically most stable surface. This finding has important consequences in surface physics. In terms of equilibrium crystal shape,[6] for instance, the surface energy anisotropy reversal means that in Pd-rich PdAg nanocrystals the relative weight of the (100) facets, compared to that of the (111) facets, is significantly higher than in Pd- and in Ag-rich PdAg particles.

In order to understand the origin of the anomalous surface stability in PdAg alloys, we investigate the role of lattice strain on the surface energy of pure fcc Ag. For this study, we used ideal bulk terminated slabs, i.e., neglected the top

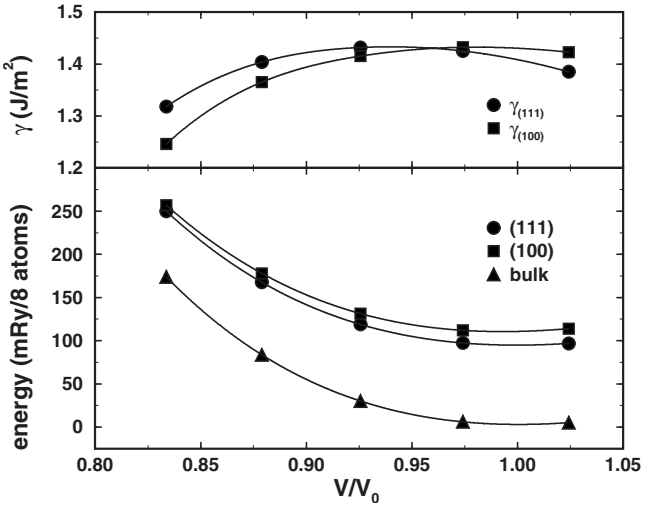

FIG. 2. Upper panel: Surface energies for the (111) and (100) surfaces of Ag as a function of volume. Lower panel: Total energies for the (111) (circles) and (100) (squares) slabs of Ag and for bulk Ag (triangles) as a function of relative volume V/V_0. V_0 is the equilibrium volume of bulk Ag.

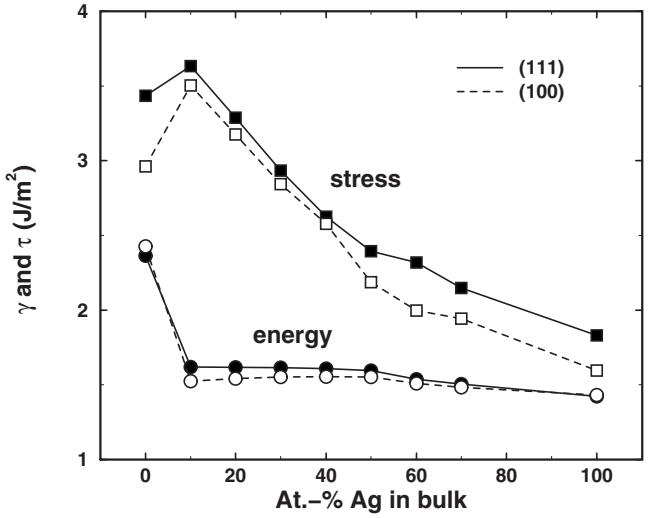

FIG. 3. Surface energy and stress for the (111) and (100) surfaces of fcc PdAg alloys as a function of bulk Ag content.

layer relaxation. In the lower panel of Fig. 2, we compare the total energies for the (111) and (100) Ag slabs and Ag bulk plotted as a function of relative volume. In this figure, the bulk energy refers to the same number of atoms as the slab energy, so the difference between the slab and bulk energies gives twice the surface energy per atom, $2\gamma A$. Since there are missing bonds in the slabs compared to the bulk, the slab "bulk" moduli are smaller than the true bulk modulus, resulting in decreasing surface energies with compression. The effect is more pronounced for the (100) facet because this facet has more broken bonds than the (111) one. This difference yields a decreasing $(\gamma A)_{100}-(\gamma A)_{111}$. When expressed per unit surface area (upper panel, Fig. 2), the surface energy difference $\Delta\gamma$ becomes negative around $V/V_0=0.96$ and reaches -35 mJ/m^2 near $V/V_0=0.884$ corresponding to the volume of pure Pd. We note that by taking into account the surface relaxation, the difference $\Delta\gamma$ would become even more negative, since relaxation decreases γ_{100} more than γ_{111}. Therefore, in pure Ag, compressive lattice strain enhances the stability of open (100) surface. The above mechanism is expected to be present in all late transition and noble metals, and we suggest that this is the main effect responsible for the stability of the (100) surface in Pd-rich alloys.

Surface stress. For the high-symmetry (111) and (100) surfaces, the surface stress was derived from the scalar Shuttleworth equation $\tau=\gamma+\partial\gamma/\partial\epsilon$, where ϵ is the in-plane lattice strain.[33,34] Equation (1) becomes cumbersome when calculating γ against lattice distortion. This can be avoided by introducing the following approximation: $\gamma \approx [E^s(c^1,c^2,c)-8E^b(\bar{c})]/(2A)$, where $\bar{c}$ is the average concentration from the slab. Note that this expression becomes exact for $c\approx 0.5$ and in the limit when the number of atomic layers from the slab tends to infinity. For the present slabs, the actual error introduced by this approximation is below the numerical accuracy of our calculations.

The calculated surface stresses are compared to the corresponding surface energies in Fig. 3. For Pd and Ag, the present surface stress values are 3.44 and 1.83 J/m^2 for the (111) facet, and 2.96 and 1.60 J/m^2 for the (100) facet. These figures are slightly larger than the former theoretical data[33] obtained using the same density functional approximation. The deviation is due to the layer relaxation neglected in Ref. 33.

For both surfaces the excess surface stress, listed also in the last columns of Table I, reaches exceptionally large values in Pd-rich alloys. In fact, similar high $|\tau-\gamma|$ has been obtained only for the (110) surface of fcc Rh (2.27 J/m^2) followed by that of Pd (1.37 J/m^2).[21] It is clear that the anomalously large surface stress in PdAg alloys is due to the homogeneous lattice strain effect discussed above in connection with the surface relaxation and surface energy. In order to see whether the obtained stress is sufficiently large for the surface reconstruction to occur, we estimate the elastic stain energy associated with surface reconstruction as[15] $E_{strain}(c)=G(c)b(c)$, where G is the shear modulus and $b=a\sqrt{2}/2$ is the Burgers vector for $Pd_{1-c}Ag_c$. For simplicity, we assume that the shear modulus varies linearly with c between $G_{Pd}=50$ GPa and $G_{Ag}=33$ GPa. Using the theoretical lattice constants (Table I), for the elastic energy we obtain 14.0, 13.5, 13.1, 12.7, and 12.3 J/m^2 for $c=0.0$, 0.1, 0.2, 0.3, and 0.4. Compared to the excess surface stress values (Table I), we find that $(\tau-\gamma)/E_{strain}>0.1$ for $0<c<0.4$. That is, according to the Cammarata model,[15] our data indicates that in Pd-rich alloys both the thermodynamically unstable (111) and the stable (100) surfaces show instability against reconstruction. This prediction is in line with the $c(2\times 2)$ patterns observed on the (100) surface of PdAg.[32]

In summary, using the PdAg system we have demonstrated that lattice strain can reverse the usual surface energy anisotropy, stabilizing an open facet relative to the close-packed surface. Furthermore, we have shown that in Pd-rich alloys, the exceptionally large surface excess stress exceeds the elastic threshold characteristic for PdAg surfaces, thus predicting mechanically unstable (111) and (100) alloy surfaces. Since there is no *a priori* reason for restricting the

disclosed phenomena to PdAg system, we conclude that a wide field of surface science and nanotechnology could substantially benefit from our discovery. In particular, the surface anisotropy reversal has significant impact in catalytic applications, where in general the open surfaces are considered to be more reactive than the close-packed ones,[3] as well as in nanopattern fabrication and surface-tailoring in metal clusters. The lattice strain-driven anomalous surface stress and surface reconstruction appear to be the most influential on the epitaxial growth of metallic and/or magnetic multilayers.[4,5] Revealing and understanding these phenomena is vital to having full control of the final performance of epitaxial heterostructures.

The Swedish Research Council, the Swedish Foundation for Strategic Research, the Academy of Finland (Contract No. 116317) and the Hungarian Scientific Research Fund (Contracts No. T046773 and No. T048827) are acknowledged for financial support. M.R., K.K., and M.P.J.P. acknowledge the computer resources of the Finnish IT Center for Science (CSC) and Mgrid project.

[1] H. Ibach, Surf. Sci. Rep. **29**, 193 (1997).
[2] D. Sander, Curr. Opin. Solid State Mater. Sci. **7**, 51 (2003).
[3] T. Bligaard and J. K. Norskov, in *Chemical Bonding at Surfaces*, edited by A. Nilsson, L. G. M. Pettersson, and J. K. Norskov (Elsevier, New York, 2007).
[4] R. F. C. Farrow, IBM J. Res. Dev. **42**, 43 (1998).
[5] J. J. Miguel and R. Miranda, J. Phys.: Condens. Matter **14**, R1063 (2002).
[6] L. Vitos, A. V. Ruban, H. L. Skriver, and K. Kollar, Surf. Sci. **411**, 186 (1998).
[7] J. Kollár, L. Vitos, B. Johansson, and H. L. Skriver, Phys. Status Solidi B **217**, 405 (2000).
[8] J. J. Métois, A. Saúl, and P. Müller, Nat. Mater. **4**, 238 (2005).
[9] J. Sokolov, F. Jona, and P. M. Marcus, Solid State Commun. **49**, 207 (1984).
[10] M. Aldén, H. L. Skriver, S. Mirbt, and B. Johansson, Phys. Rev. Lett. **69**, 2296 (1992).
[11] M. Aldén, H. L. Skriver, S. Mirbt, and B. Johansson, Surf. Sci. **315**, 157 (1994).
[12] P. Müller and A. Saúl, Surf. Sci. Rep. **54**, 157 (2004).
[13] S. K. Kwon, Z. Nabi, K. Kádas, L. Vitos, J. Kollár, B. Johansson, and R. Ahuja, Phys. Rev. B **72**, 235423 (2005).
[14] C. Herring, *The Physics of Powder Metallurgy*, edited by W. E. Kingston (McGraw-Hill, New York, 1951).
[15] R. C. Cammarata, Prog. Surf. Sci. **46**, 1 (1994).
[16] P. Hohenberg and W. Kohn, Phys. Rev. **136**, B864 (1964).
[17] J. P. Perdew and Y. Wang, Phys. Rev. B **45**, 13244 (1992).
[18] D. M. Ceperley and B. J. Alder, Phys. Rev. Lett. **45**, 566 (1980).
[19] J. P. Perdew, J. A. Chevary, S. H. Vosko, K. A. Jackson, M. R. Pederson, D. J. Singh, and C. Fiolhais, Phys. Rev. B **46**, 6671 (1992).
[20] W. Liu, X. Liu, W. T. Zheng, and Q. Jiang, Surf. Sci. **600**, 257 (2006).
[21] L. Vitos, in *Computational Quantum Mechanics for Materials Engineers: The EMTO Method and Applications*, Engineering Materials and Processes Series (Springer-Verlag, London, 2007).
[22] L. Vitos, H. L. Skriver, B. Johansson, and J. Kollár, Comput. Mater. Sci. **18**, 24 (2000).
[23] L. Vitos, Phys. Rev. B **64**, 014107 (2001).
[24] O. K. Andersen, O. Jepsen, and G. Krier, in *Lectures on Methods of Electronic Structure Calculation* (World Scientific, Singapore, 1994), p. 63.
[25] P. Soven, Phys. Rev. **156**, 809 (1967).
[26] B. L. Györffy, Phys. Rev. B **5**, 2382 (1972).
[27] L. Vitos, I. A. Abrikosov, and B. Johansson, Phys. Rev. Lett. **87**, 156401 (2001).
[28] In the self-consistent calculations, the one-electron equations were solved within the scalar relativistic and soft core approximations. The EMTO Green's function was calculated for 16 energy points. We used *s*, *p*, *d*, and *f* EMTO orbitals. In the irreducible part of the surface and bulk Brillouin zones we used 160 and 240 *k*-points, respectively. The total charge density was expanded in spherical harmonics, including terms up to $l_{max}=10$.
[29] S. Müller and A. Zunger, Phys. Rev. Lett. **87**, 165502 (2001).
[30] A. V. Ruban, S. I. Simak, P. A. Korzhavyi, and B. Johansson, Phys. Rev. B **75**, 054113 (2007).
[31] M. Ropo, Phys. Rev. B **74**, 195401(4) (2006).
[32] P. T. Wouda, M. Schmid, B. E. Nieuwenhuys, and P. Varga, Surf. Sci. **417**, 292 (1998).
[33] J. Kollár, L. Vitos, J. M. Osorio-Guillén, and R. Ahuja, Phys. Rev. B **68**, 245417 (2003).
[34] The surface stress was calculated from the difference between the slope of the slab energy $E^s(c^1,c^2,c)$ and the bulk energy $E^b(\bar{c})$ calculated as a function of small in-plane lattice distortion $\epsilon=0,\pm0.01$ and ±0.02. Further details about the stress calculations are presented elsewhere (Ref. 33).